Rovibrational spectra of LiH2+, LiHD+ and LiD2+ determined from FCI property surfaces

ARTICLE *in* THE JOURNAL OF PHYSICAL CHEMISTRY A · MAY 2007

Impact Factor: 2.69 · DOI: 10.1021/jp066369d · Source: PubMed

2 AUTHORS, INCLUDING:

Alister J Page
University of Newcastle
57 PUBLICATIONS **650** CITATIONS

Rovibrational Spectra of LiH_2^+, $LiHD^+$ and LiD_2^+ Determined from FCI Property Surfaces

Alister J. Page and Ellak I. von Nagy-Felsobuki*

The Molecular Structure and Detection Group, School of Environmental and Life Sciences, The University of Newcastle, Callaghan, NSW 2308 Australia

Received: September 28, 2006; In Final Form: March 15, 2007

Full configuration interaction (FCI) has been used in conjunction with the lithium [6s5p3d1f] (Iron, M. A.; et al. *Mol. Phys.* **2004**, *101*, 1345) and hydrogen aug-cc-pVTZ basis sets to construct an 83-point potential energy surface of the $^1A_1$ ground state of $^7LiH_2^+$. Vibrational and rovibrational wave functions of the $^{6,7}LiH_2^+$, $^{6,7}LiHD^+$, and $^{6,7}LiD_2^+$ ground states were calculated variationally using an Eckart−Watson Hamiltonian. For $^7LiD_2^+$, rovibrational transition frequencies for $K = 0$, 1, 2 and $J \leq 10$ are within ca. 0.1% of recent experimental values (Thompson, C. D.; et al. *J. Chem. Phys.* **2006**, *125*, 044310). A 47-point FCI dipole moment surface was embedded in the rovibrational Hamiltonian to calculate vibrational and rovibrational radiative properties. At 296 K, with $v \leq 4$ and $J \leq 4$, the $2_{02} \leftarrow 3_{03}$ rotational transition in the $|001\rangle$ band was found to have the greatest spectral intensity with respect to the ground electronic states of $^{6,7}LiH_2^+$, $^{6,7}LiHD^+$, and $^{6,7}LiD_2^+$. In each case, the most intense rovibrational transitions have been assigned unequivocally using the J, K_a, K_c assignment scheme.

1. Introduction

According to current mechanisms of interstellar radiative cooling, primordial lithium chemistry was involved in the onset of the stellar evolution of the universe.[1,2] The ubiquity of atomic hydrogen throughout the early (and present) universe suggests that primordial Li and Li^+ chemistry would be dominated by formation and decomposition reactions of lithium hydrides.[3] For instance, photochemical processes such as

$$Li + H \rightarrow LiH + h\nu$$

$$Li^+ + H \rightarrow LiH^+ + h\nu$$

$$Li^+ + H^- \rightarrow LiH + h\nu$$

and similarly

$$LiH^+ + H \rightarrow Li^+ + H_2$$

$$LiH + H^+ \rightarrow Li + H_2^+$$

$$LiH^+ + H \rightarrow Li^+ + H + H$$

would be suitable candidates for nascent Li−H interactions. Reactions of this nature have been extensively investigated by Gianturco and co-workers.[1,3−6]

The Li^+−H_2 collision complex is produced from the anisotropic interaction between Li^+ and H_2 and possesses a binding energy of ca. 0.28 eV.[7,8] It is therefore not surprising that the nature of the scattering collision between Li^+ and H_2 has been the subject of many theoretical investigations.[3−7,9−22] In particular, such investigations have focused on the potential energy surface (PES) of the ground electronic state ($^1A_1$) of LiH_2^+. For example, Lester[18,19] has constructed a 150-point ab initio PES using Hartree−Fock self-consistent field (HF-SCF) theory, employing the Li and H atomic orbital (AO) basis sets of Huzinaga.[23] Russek et al.[11] have calculated a 120-point HF-SCF surface for their classical trajectory studies involving the Li^+−D_2 collision complex. Kutzelnigg et al.[24] have highlighted that the intra electron correlation within the H_2 fragment was not constant for collinear Li^+−H_2 collisions and so noted that the PES of Lester[18,19] and Russek et al.[11] may be deficient where dissociative collisions were possible. Furthermore, Kutzelnigg et al.[24] incorporated electron correlation using the paired natural orbital-independent electron pair approximation (PNO-IEPA) ansatz to construct a 300-point PES. Kochanski[16] included electron correlation via the use of an Epstein−Nesbet partition of molecular Hamiltonians that incorporated a double perturbation scheme. Kochanski also calculated polarization energies for a number of molecular geometries. As neither of the methods employed by Kutzelnigg et al.[24] or Kochanski[16] were variational, Searles and von Nagy-Felsobuki[7] calculated a 170-point PES using configuration interaction, which included all single and double excitations (CISD). More recently, Gianturco and co-workers[3−6] have employed multireference valence bond (MRVB) and MRCI theory in the construction of a ground state PES, to elucidate the nature of the reaction dynamics present in the Li^+−H_2 collision complex. Though the electron correlation methods outlined here vary, there is common agreement that the ground electronic state of LiH_2^+ possesses C_{2v} symmetry, with a bond angle and bond length of approximately 21° and 2.0 Å, respectively. No full configuration interaction (FCI) PES or dipole moment surface (DMS) of the ground electronic state of LiH_2^+ has been reported to date, even though such calculations are now tractable even for methodologies employing large single particle basis sets.

Investigations dealing with the rovibrational structure of lithium−hydrogen systems are rare. For instance, Gianturco and co-workers[1] have performed calculations to determine the bound vibrational and rovibrational states of the LiH and LiH^+ ground states as well as frequency and transition intensity data for all bound state transitions. More recently, these workers have extended their study to the LiH_2^+ complex, reporting several J

* Author to whom all correspondence should be sent. E-mail: ellak@newcastle.edu.au. Fax: +61-2-49216923. Tel: ++61-2-49215482.

10.1021/jp066369d CCC: $37.00
Published on Web 04/25/2007

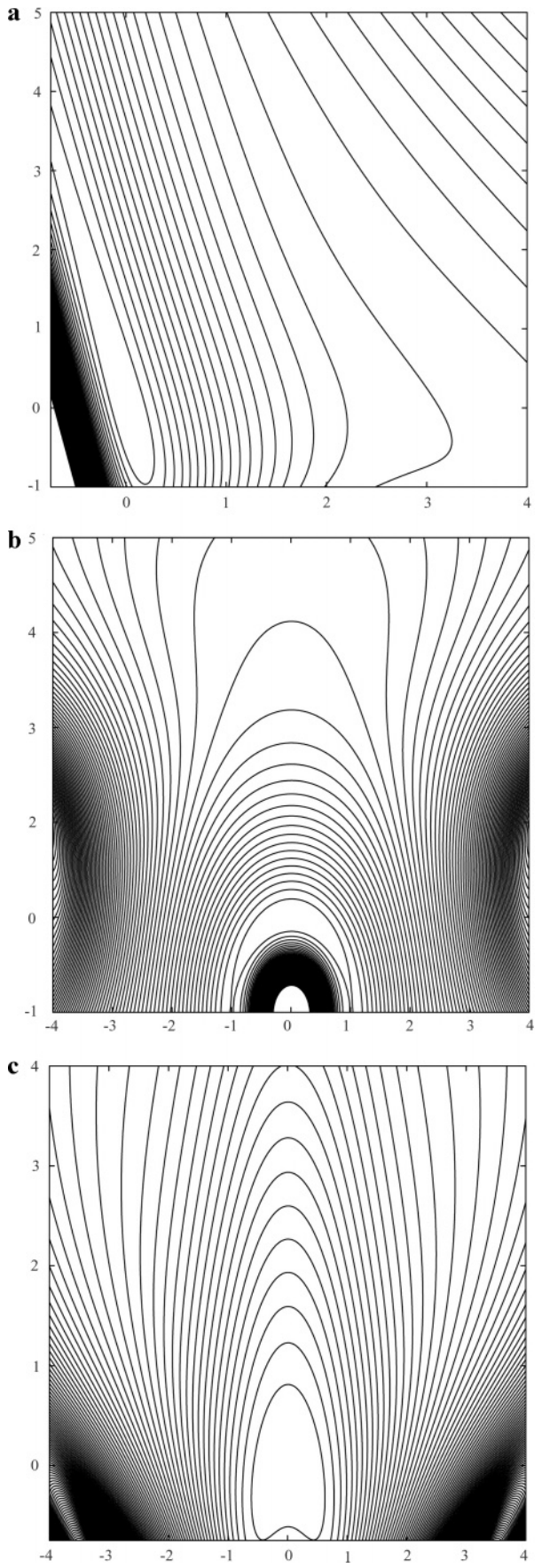

Figure 1. Two-dimensional normal-mode projections of the Ogilvie $P(5,5)$ $^7LiH_2^+$ ground state potential energy function (in au): (a) bend mode (*x*-axis) versus breathe mode (*y*-axis); (b) asymmetric stretch mode (*x*-axis) versus breathe mode (*y*-axis); (c) asymmetric stretch mode (*x*-axis) versus bend mode (*y*-axis). Contours are spaced at 25 kJ mol^{-1}.

TABLE 1: Comparison of Theoretical and Experimental Properties of Li^+, $^7LiH^+$, ^7LiH and H_2

	Li^+			
	IE_1/eV	$^1S_0 \leftarrow {}^3S_1$/eV	$^1S_0 \leftarrow {}^3P_J^0$/eV	α/a_0^3
this work[a]	75.566	59.319	61.423	0.166
experiment[b]	75.640	59.021	61.282	0.192[c]
	$^7LiH^+$			
	R_e/Å	D_e/eV	ZPE/cm^{-1}	μ_e/D
this work[a]	2.199	0.136	220.5	0.737
Magnier[c]	2.196	0.130	208.5	0.702
	^7LiH			
	R_e	D_e/eV	ZPE/cm^{-1}	μ_e/D
this work [a)]	1.601	2.479	697.7	6.012
experiment	1.59[d]	2.515[e]	697.8[f]	5.881[g]
	H_2			
	R_e/Å	D_e/eV	ZPE/cm^{-1}	
this work[a]	0.743	4.707	2200.3	
Experiment[h]	0.741	4.478	2200.6	

[a] All calculations in this work employed FCI with the Li CVTZ and H aug-cc-pVTZ basis sets. [b] Reference 35. [c] Reference 36. [d] Reference 37. [e] Reference 44. [f] Reference 38. [g] Reference 39. [h] Reference 40.

$= 0$ bound states computed using a multireference PES.[4] Xiao and Poirier[25] have recently calculated all bound and resonant rovibrational states of the weakly bound $Li^-(H_2)$ electrostatic complex. Also, the cross-sections for rotationally inelastic collisions of LiH with helium and the vibrational excitation and relaxation rate constants of the He−LiH system have been computed by Taylor and Hinde.[26,27] Vibrational transition frequencies and intensities of the $J = 0$ states of LiH_2^+ have also been reported by Bulychev et al.,[22] who employed a PES constructed at the MP2 level of theory. Recent rovibrational measurements of LiD_2^+ by Bieske and co-workers[28] suggest that theoretical calculations of the rovibrational spectra of LiH_2^+ and its isotopomers would be timely.

We extend the previous investigation of $^7LiH_2^+$ by Searles and von Nagy-Felsobuki[7] and report a FCI discrete PES and DMS for the ground electronic state of $^7LiH_2^+$. Furthermore, the corresponding analytical representations will be presented to calculate ab initio vibrational band origins, rovibrational transition energies, optical vibrational radiative properties, and rovibrational absorption intensities of the $^{6,7}LiH_2^+$, $^{6,7}LiHD^+$, and $^{6,7}LiD_2^+$ ground states.

2. Details of Computational Electronic Structure

Unless stated otherwise, ab initio calculations reported below employed the FCI level of theory[29,30] as implemented in the MOLPRO 2002.6 program system.[31] All electrons were included in the FCI wave functions.

In the construction of ab initio discrete property surfaces, it is necessary to employ large single particle basis sets that included high angular momentum functions. It is also necessary to keep the cardinality of these basis sets "modest" due to the escalating size of the FCI matrix. In a recent study,[32] we have employed an augmented version of the quadruple-ζ core-valence basis set (denoted CVQZ) for beryllium.[33] It was shown that this basis set successfully modeled the atomic properties (pertinent to helium bonding) of beryllium and its monocation to a high degree of accuracy with relative efficiency. As such, the [6s5p3d1f] core-valence triple-ζ (CVTZ) basis set[33] was used

TABLE 2: *P*(5,5) OGL Potential Energy Function of the $^1A_1$ Ground State of $^7LiH_2^+$ [a]

	expansion coefficient			expansion coefficient	
expansion term	numerator	denominator	expansion term	numerator	denominator
1	−8.45927025	1.0	$\rho_1\rho_3^3 + \rho_2\rho_3^3$	−0.48683512	−0.04225458
$\rho_1 + \rho_2$	−0.35389318	−0.04182015	$\rho_1^2\rho_2^2$	−0.91368539	−0.11574730
ρ_3	7.44788829	0.88041016	$\rho_1^2\rho_3^2 + \rho_2^2\rho_3^2$	0.68407066	0.07702247
$\rho_1^2 + \rho_2^2$	−0.32568099	−0.05001609	$\rho_1^2\rho_2\rho_3 + \rho_1\rho_2^2\rho_3$	−0.35578126	−0.04157243
ρ_3^2	−0.50381694	−0.10126124	$\rho_1\rho_2\rho_3^2$	−1.02203185	−0.11737412
$\rho_1\rho_2$	−0.61305103	−0.06228294	$\rho_1^5 + \rho_2^5$	0.35384341	0.04218390
$\rho_2\rho_3 + \rho_1\rho_3$	2.85791912	0.33864751	ρ_3^5	−0.31153258	−0.03004235
$\rho_1^3 + \rho_2^3$	−0.91065426	−0.09651928	$\rho_1^4\rho_2 + \rho_1\rho_2^4$	−1.60778172	−0.18455140
ρ_3^3	−2.66822302	−0.25257287	$\rho_1^4\rho_3 + \rho_2^4\rho_3$	−0.09777925	−0.00882831
$\rho_1^2\rho_2 + \rho_1\rho_2^2$	0.29927973	0.03978290	$\rho_1\rho_3^4 + \rho_2\rho_3^4$	0.28490058	0.02591631
$\rho_1^2\rho_3 + \rho_2^2\rho_3$	0.86255212	0.11253631	$\rho_1^3\rho_2^2 + \rho_1^2\rho_2^3$	0.85707053	0.10305730
$\rho_1\rho_3^2 + \rho_2\rho_3^2$	0.29796945	0.03375714	$\rho_1^3\rho_3^2 + \rho_2^3\rho_3^2$	−1.39616596	−0.17137605
$\rho_1\rho_2\rho_3$	−2.20075520	−0.28352726	$\rho_1^2\rho_3^3 + \rho_2^2\rho_3^3$	0.78176183	0.09533249
$\rho_1^4 + \rho_2^4$	−0.86984179	−0.11424443	$\rho_1^3\rho_2\rho_3 + \rho_1\rho_2^3\rho_3$	2.23376160	0.26369189
ρ_3^4	0.50819733	0.02309842	$\rho_1\rho_2\rho_3^3$	−1.59243883	−0.19373458
$\rho_1^3\rho_2 + \rho_1\rho_2^3$	2.48456329	0.29230210	$\rho_1^2\rho_2^2\rho_3$	−1.44860717	−0.17276139
$\rho_1^3\rho_3 + \rho_2^3\rho_3$	−0.99427325	−0.11856066	$\rho_1^2\rho_2\rho_3^2 + \rho_1\rho_2^2\rho_3^2$	0.52513712	0.06628911

$(\chi^2)^{1/2} = 2.4 \times 10^{-5}\ E_h$

[a] The OGL expansion variable is defined in the text; see eq 1. $\sigma_{67} = 0$ using SVD analysis.

TABLE 3: Dipole Moment Function of the $^1A_1$ Ground State of $^7LiH_2^+$ Employing Internal Displacement Coordinates[a]

μ_y ($C_{ijk} = C_{jik}$)				μ_x ($C_{ijk} = -C_{jik}$)			
term	expansion coeffficient	term	expansion coeffficient	term	expansion coeffficient	term	expansion coeffficient
C_{000}	5.7600573−01	C_{220}	−9.4638212−02	C_{100}	1.8861389−01	C_{302}	−1.1685479−02
C_{100}	3.4803935−05	C_{202}	−1.6226037−02	C_{200}	2.0762683−03	C_{311}	−2.4482756−03
C_{001}	1.8903464−01	C_{112}	2.1410803−01	C_{101}	−4.7736208−03	C_{212}	−2.4610882−02
C_{200}	4.7606581−01	C_{103}	2.1318544−03	C_{300}	−5.2909276−02	C_{203}	2.7818015−02
C_{110}	4.9100126−05	C_{004}	9.5231394−01	C_{210}	−2.4305515−02	C_{104}	−2.7099083−02
C_{101}	5.3544358−02	C_{500}	8.2285918−10	C_{201}	1.6578283−02	C_{600}	1.6355912−06
C_{002}	−1.1175649−02	C_{410}	2.6331849−07	C_{102}	6.0458961−02	C_{510}	1.6918581−04
C_{300}	−5.9662817−03	C_{401}	−3.7634788−05	C_{400}	−1.3196973−02	C_{501}	−1.5989614−03
C_{210}	2.7336005−04	C_{320}	−2.9354169−04	C_{310}	−1.9791243−02	C_{420}	−1.1817353−02
C_{201}	1.5930731−02	C_{302}	−3.8223416−02	C_{301}	−1.4452518−02	C_{402}	6.6304732−03
C_{111}	6.1168562−06	C_{311}	−2.7397681−04	C_{211}	−1.1476566−03	C_{411}	−1.7545946−03
C_{102}	−6.0344463−02	C_{203}	−1.2935224−04	C_{202}	1.9868723−02	C_{321}	−1.1987818−02
C_{003}	−4.3103153−01	C_{221}	4.9197286−02	C_{103}	1.0787918−02	C_{312}	−5.0469810−05
C_{400}	−4.4141602−06	C_{212}	−1.0932027−07	C_{500}	2.9653075−03	C_{303}	1.8401925−02
C_{310}	2.4547978−02	C_{113}	−4.0974165−01	C_{410}	−1.0367889−02	C_{204}	−2.9647557−02
C_{301}	2.7332238−02	C_{104}	8.7353476−03	C_{401}	4.2567467−03	C_{213}	1.8879820−02
C_{211}	−1.2784771−05	C_{005}	−2.6951120−03	C_{320}	5.0693164−03	C_{105}	3.4407226−02
$(\chi^2)^{1/2} = 5.5 \times 10^{-3}$				$(\chi^2)^{1/2} = 1.9 \times 10^{-9}$			

[a] 5.7600573−01 denotes 5.7600573×10^{-1}.

for lithium, and the augmented correlation-consistent triple-ζ (aug-cc-pVTZ) basis set[34] was used for hydrogen.

To justify the use of the Li CVTZ and H aug-cc-pVTZ basis sets, atomic properties of Li^+ including the first ionization energy (IE_1), electronic transition energies and electric dipole polarizability (α) were calculated and compared with experimental values. Molecular properties of LiH, LiH^+, and H_2 such as the equilibrium geometry (R_e), dissociation energy (D_e), zero-point energy (ZPE), and equilibrium dipole moment (μ_e) were also calculated and compared with experiment. These comparisons are given in Table 1. In cases where experimental data was not available, results in Table 1 are compared with the most accurate theoretical data that is currently available in the literature.

From Table 1, the FCI IE_1 and α of Li^+ differed from experiment [35] by −0.074 eV and −0.026 a_0^3, respectively. The FCI $^1S_0 \leftarrow {}^3S_1$ and $^1S_0 \leftarrow {}^3P_J^0$ transitions of Li^+ were 0.298 and 0.141 eV higher than the respective experimental values.[35] It should be noted that the FCI IE_1 for the lithium atom differed by −0.013 eV from the experimental value,[35] and the observed $^2S_{1/2} \leftarrow {}^2P_J^0$ transition energy of Li was 0.003 eV[35] lower than the FCI value using the CVTZ basis set.

No experimental values of R_e, D_e, ZPE, or μ_e for $^7LiH^+$ were found in the literature. In Table 1 the FCI values for this ion are therefore compared to the recent theoretical values of Magnier[36] and are observed to be in excellent agreement. For instance, the R_e, ZPE and μ_e for $^7LiH^+$ differed by 0.003 Å, 0.006 eV, 12.0 cm^{-1}, and 0.035 D, respectively. Similarly, the R_e, ZPE, and μ_e values of ^7LiH using FCI compared favorably with experiment, differing by 0.005 Å,[37] −0.1 cm^{-1},[38] and 0.131 D,[39] respectively. The FCI/CVTZ equilibrium bond length and ZPE of H_2 were also in excellent agreement with experiment, differing from the respective experimental values[40] by 0.002 Å and −0.3 cm^{-1}.

From Table 1 it is also seen that the FCI D_e value of $^7LiH^+$ is 0.136 eV (for the $\{(^1S)Li^+ + (^2S)H\}$ dissociation channel), 0.006 eV higher than that of Magnier.[36] However, the dissociation energy reported in this work was in closer agreement with other recent calculations (for instance 0.140,[41] 0.141,[42] and 0.140 eV).[43] For LiH, D_e calculated using FCI (for the $\{(^2S)Li +$

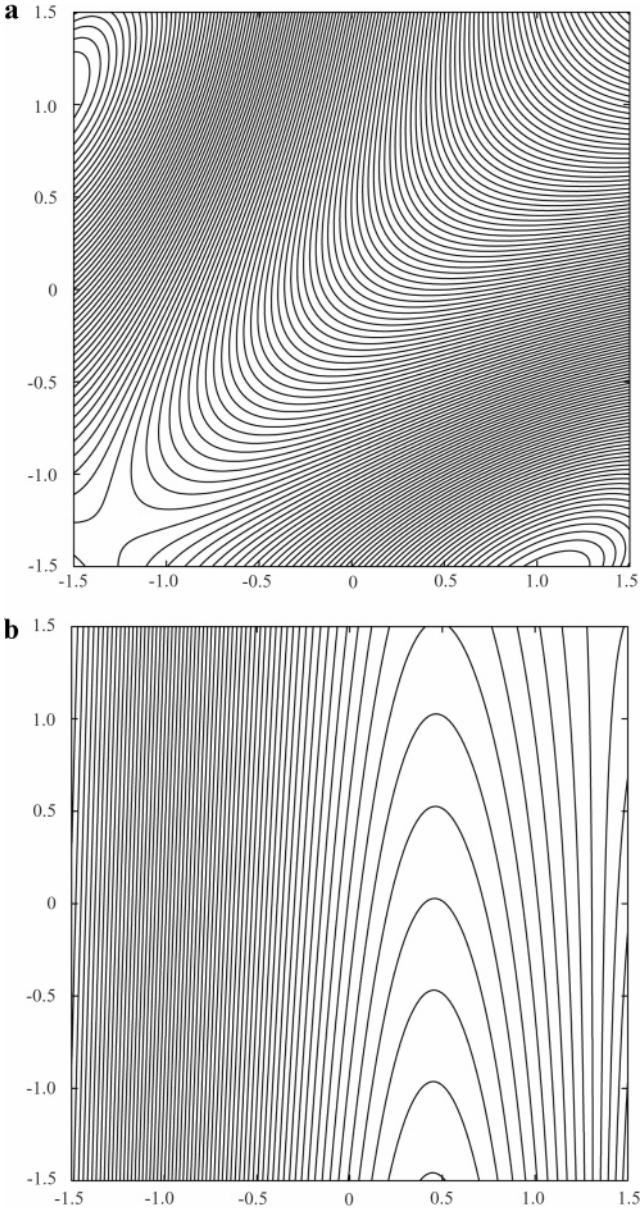

Figure 2. Two-dimensional constant dipole projections of μ_y for the $^7LiH_2^+$ ground state using the fifth-order expansion of internal displacement coordinates: (a) ρ_2 (*x*-axis) versus ρ_1 (*y*-axis); (b) ρ_3 (*x*-axis) versus ρ_2 (*y*-axis). Contours are spaced at 6.0×10^{-3} au.

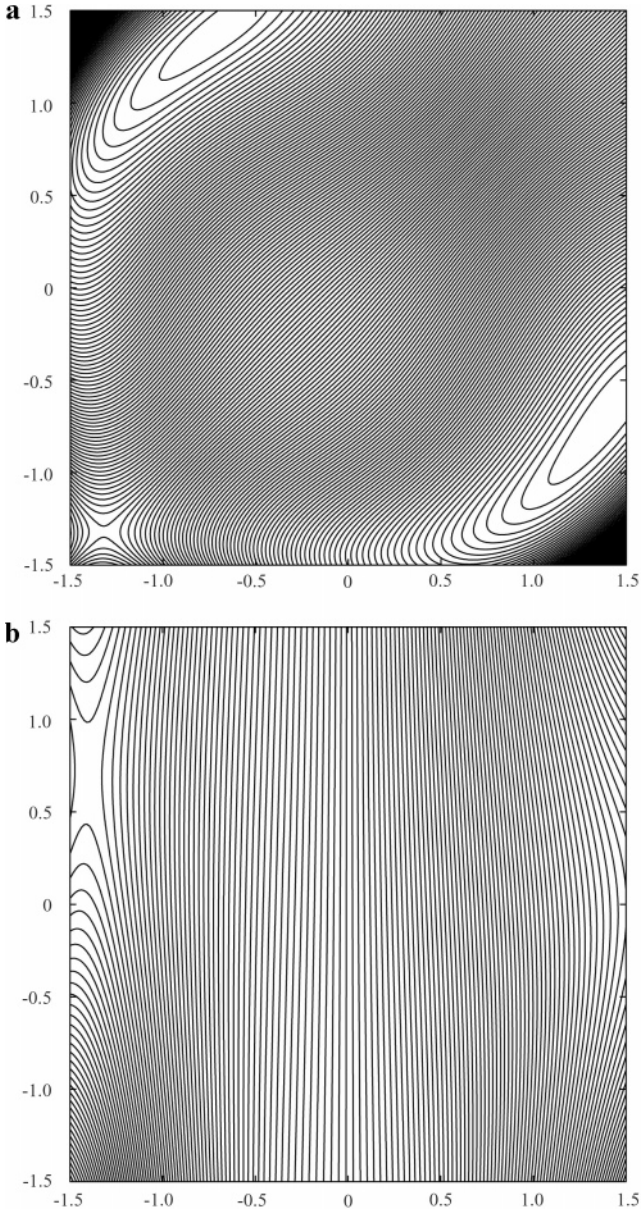

Figure 3. Two-dimensional constant dipole projections of μ_x for the $^7LiH_2^+$ ground state using the sixth-order expansion of internal displacement coordinates: (a) ρ_2 (*x*-axis) versus ρ_1 (*y*-axis); (b) ρ_3 (*x*-axis) versus ρ_1 (*y*-axis). Contours are spaced at 2.0×10^{-3} au.

(^{2}S)H} dissociation channel) was 0.036 eV lower than experiment.[44] The difference between FCI/aug-cc-pVTZ and experimental[40] D_e values of H_2 for the dissociation channel {(^{2}S)H + (^{2}S)H} was more pronounced, being 0.229 eV. Nevertheless, the $D_e(H_2)$ value calculated in this work was in closer agreement with experiment than recent theoretical calculations of Yang et al.,[45] who employed a MRCI ansatz using the aug-cc-pV6Z basis set.[34,46−49] Their calculated $D_e(H_2)$ was 4.7105 eV, a value differing from experiment by 0.232 eV. These workers have stated that all theoretical values of $D_e(H_2)$ reported in the literature generally differed from the experimental value by approximately 6%.

The accuracy of the triple-ζ basis sets employed here was also investigated with respect to the $^7LiH_2^+$ ground state. Using FCI, the $^7LiH_2^+$ $^1A_1$ ground state was found to have an equilibrium bond length and angle of 2.027 Å and 21.4°, respectively. These values agree well with the recent theoretical values of 2.034 Å and 21.3°, which were calculated using the coupled-cluster with single and double excitations (CCSD) ansatz.[10] The potential well-depth (D_e) with respect to the {(^{1}S)Li^+ + ($^1\Sigma_g^+$)H_2} dissociation channel was calculated to be 0.266 eV. This well-depth agreed favorably with the previously calculated values of 0.263 eV (MP2), 0.255 eV (CCSD),[10] and 0.258 eV (CISD).[7] With respect to experiment, the D_0 has been measured to be 0.282 ± 0.199 eV,[8] and so any comparison with the corresponding experimental D_e and these calculated values would be futile, due to the magnitude of error in the measurement.

Using the all-electron CCSD(T) ansatz (as implemented in GAMESS[50]) with the triple-ζ basis sets employed in the present work, the breathe (a_1 symmetry), bend (a_1 symmetry) and asymmetric stretch (b_2 symmetry) harmonic frequencies of the $^7LiH_2^+$ ground state were 488.8, 4281.4, and 708.9 cm^{-1}, respectively. The approximation of uncoupled normal modes was also employed to calculate FCI fundamental anharmonic frequencies of $^7LiH_2^+$. It was found that the breathe, bend, and asymmetric stretch fundamental vibration frequencies were

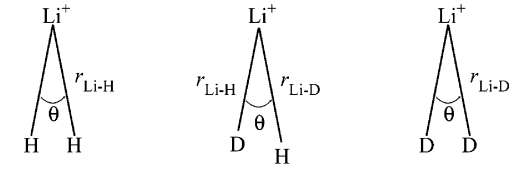

$r_{Li-H} = 2.089$Å, $\theta = 23.4°$ | $r_{Li-H} = 2.100$Å, $r_{Li-D} = 2.096$Å, $\theta = 20.6°$ | $r_{Li-H} = 2.094$Å, $\theta = 20.6°$

Figure 4. Average equilibrium structures of $^7LiH_2^+$, $^7LiHD^+$, and $^7LiD_2^+$ in the ground vibrational state, using the Ogilvie $P(5,5)$ $^7LiH_2^+$ ground state potential energy function.

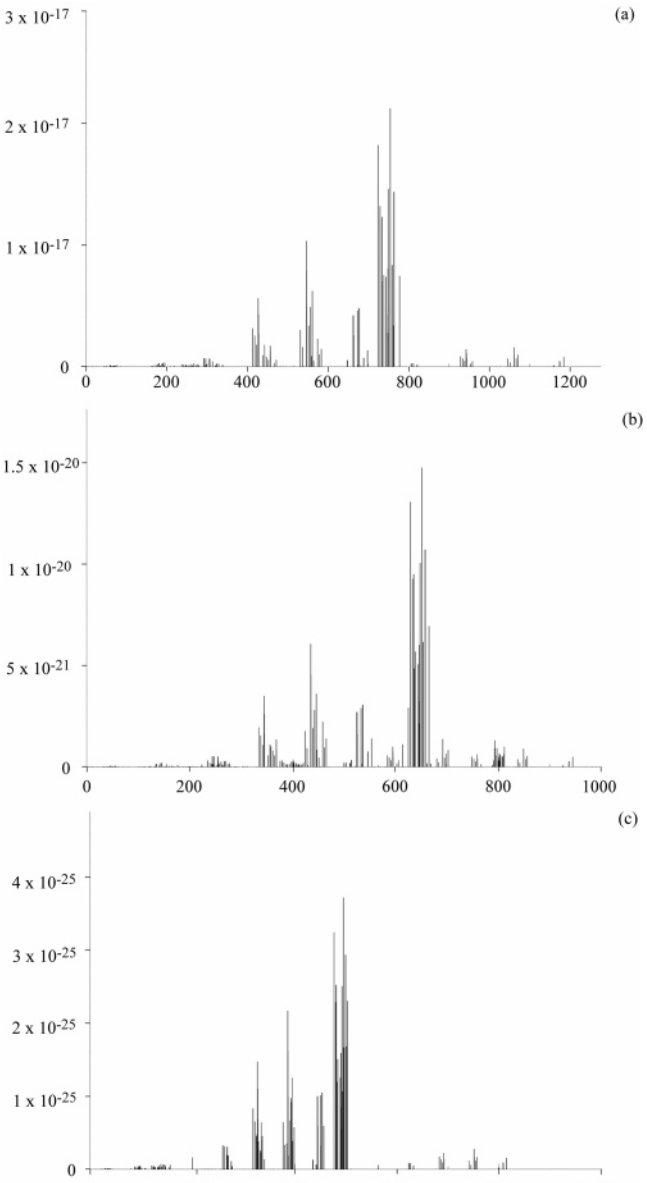

Figure 5. Comparison of ab initio rovibrational spectra at 296 K: (a) $^7LiH_2^+$ ground state, 305 transitions shown; (b) $^7LiHD^+$ ground state, 514 transitions shown; (c) $^7LiD_2^+$ ground state, 233 transitions shown. All transitions are such that $v \leq 4$, $J \leq 4$ and $S_{ab} \geq 1.0 \times 10^{-30}$ cm molecule^{-1}. All line positions given in cm^{-1}, all line intensities given in cm molecule^{-1}.

487.7, 2058.9, and 486.1 cm^{-1}, respectively. The pronounced differences in the latter two modes were attributed to the differences in the curvatures of the FCI and CCSD(T) 1D potential energy surfaces.

3. FCI Property Surfaces

3a. FCI Discrete Potential Energy Surface and Analytical Representation. The FCI discrete PES for the $^1A_1$ ground state of $^7LiH_2^+$ was constructed using an iterative procedure, which has been documented extensively elsewhere.[51−53] The discrete FCI PES of $^7LiH_2^+$ ultimately consisted of 83 points within the domains $1.69394\ a_0 \leq R_{H-Li} \leq 7.03561\ a_0$, $0.61825\ a_0 \leq R_{Li-H} \leq 7.03561\ a_0$, and $0.50231\ a_0 \leq R_{H-H} \leq 5.58752\ a_0$. The lower and upper bounds of the PES in this domain were −8.4592693576 and −6.8369494113 E_h, respectively. The full discrete FCI PES can be obtained from the electronic archive.[54] The potential energy function (PEF) was required to predict physical properties of the molecule and provide chemical accuracy over the domain of interest. The latter was gauged using the square root of the residual error, $(\chi^2)^{1/2}$, of the PEF. The most satisfactory analytical representation in terms of these criteria was the $P(5,5)$ Padé function of the Ogilvie (OGL) expansion variable, with the singular value σ_{67} set to zero using singular value decomposition (SVD) analysis. The OGL expansion variable is defined as

$$\rho_i^{OGL} = \frac{2(R_i - R_i^{equil})}{R_i + R_i^{equil}} \tag{1}$$

where R_i and R_i^{equil} are instantaneous and equilibrium bond lengths, respectively.[55] The $(\chi^2)^{1/2}$ value of the OGL $P(5,5)$ PEF was 2.4×10^{-5} E_h, indicating that this function is of spectroscopic accuracy over the domain of interest. By restricting both n and m to 5, it was possible to ensure that the variationally optimized term coefficients of the PEF were unique. These coefficients are detailed in Table 2. Figure 1 shows 2D constant energy contour plots of the OGL $P(5,5)$ PEF in terms of the three rectilinear vibrational coordinates.[56]

3b. FCI Discrete Dipole Moment Surface and Analytical Representation. A 47-point FCI discrete DMS of the $^1A_1$ ground state of $^7LiH_2^+$ was constructed and is available from the electronic archive.[54] The molecule was held in the Eckart frame[57] for all points on the discrete grid. The origin of the dipole moment function was placed at the center-of-mass of the molecule. Thus, μ_y was coincident with the (positive) vector from the origin to the Li nucleus, and μ_z was necessarily identically zero. At the equilibrium geometry, μ_y was found to be 0.5750 au. The discrete DMS included points within the domains $2.53501\ a_0 \leq R_1 \leq 5.97269\ a_0$, $0.61825\ a_0 \leq R_2 \leq 5.49285\ a_0$, and $5.39577° \leq \theta \leq 91.05387°$. The minimum values of the μ_y and μ_x components of the dipole moment over this region were +0.0667 and −0.2372 au, respectively, and the maximum values were 1.1973 and 0.2048 au, respectively.

In fitting the discrete DMS, power series expansions of internal displacement coordinates ($\rho_{1,2} = R_{1,2} - R_{1,2}^{equil}$ and $\rho_3 = \theta - \theta^{equil}$) were employed in the manner described by Gabriel et al.[58] As is the case with the analytical PEFs, the analytical representation of a discrete DMS must provide chemical accuracy in the dipole moment value, while predicting physically realistic properties of the molecular system over the domain of interest.[59] An appropriate DMF would thus be expected to show little electrical anharmonicity in the immediate neighborhood of the equilibrium geometry. The most satisfactory representations of the discrete μ_y and μ_x DMS components were the fifth- and sixth-order power series expansions, having $(\chi^2)^{1/2}$ values of 5.5×10^{-3} and 1.9×10^{-9} au, respectively. In both cases, no artifacts (that is singularities, etc.) were visible in the dipole moment throughout the integration domain, and so no further

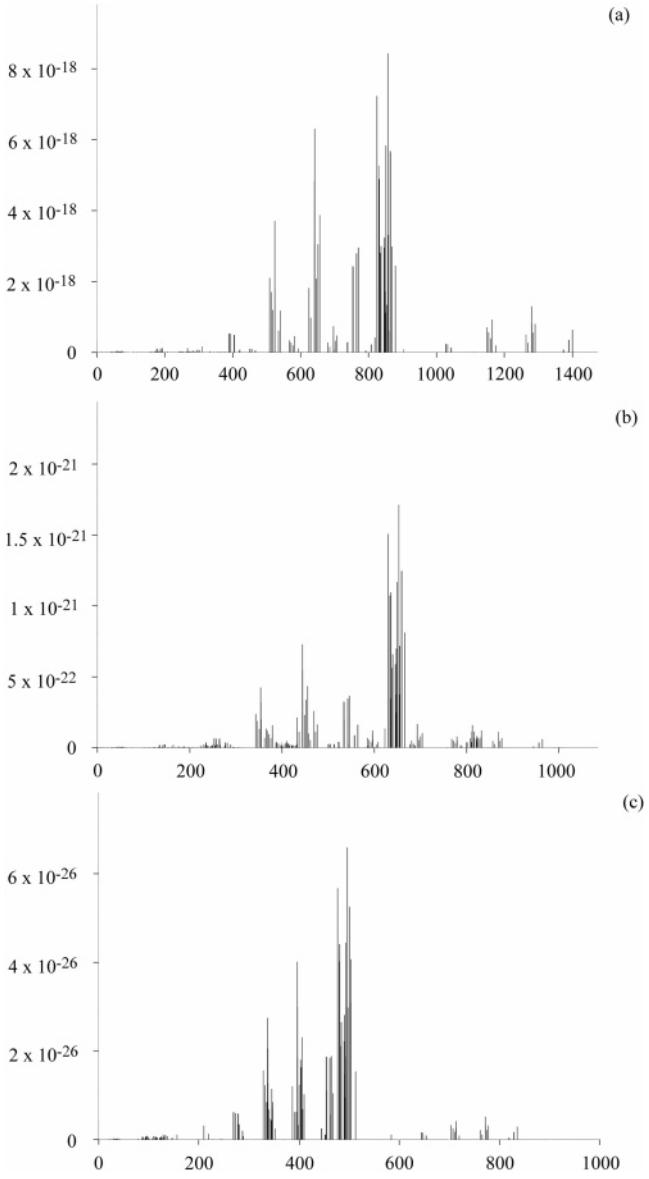

Figure 6. Comparison of ab initio rovibrational spectra at 296 K: (a) $^6LiH_2^+$ ground state, 302 transitions shown; (b) $^6LiHD^+$ ground state, 507 transitions shown; (c) $^6LiD_2^+$ ground state, 215 transitions shown. All transitions are such that $v \leq 4$, $J \leq 4$ and $S_{ab} \geq 1.0 \times 10^{-30}$ cm molecule^{-1}. All line positions given in cm^{-1}, all line intensities given in cm molecule^{-1}.

SVD analysis of the DMFs was necessary. By restricting the expansions to fifth- and sixth-order in the respective dipole moment components, it was possible to ensure that the term coefficients of the expansions were uniquely defined. The term coefficients of the analytical μ_y and μ_x DMFs are given in Table 3. Two-dimensional constant dipole projections of the analytical μ_y and μ_x DMFs are shown in Figure 2 and Figure 3, respectively. The contour spacing shown in Figures 2 and 3 were chosen so that good indications of the topology of the DMF over the integration domain were obtained.

4. Ab Initio Rovibrational States

4a. Vibrational Band Origins and Rovibrational Transition Energies. The C_{2v} coordinate rovibrational Hamiltonian of Carney et al.[56] was employed for the calculation of vibrational states. Using matrix notation, this Hamiltonian is of form

$$H_{ij}^{VR} = E_i\langle S\rangle_{ij} + \frac{1}{2}\langle A\rangle_{ij}\hat{\Pi}_x^2 + \frac{1}{2}\langle B\rangle_{ij}\hat{\Pi}_y^2 + \frac{1}{2}\langle C\rangle_{ij}\hat{\Pi}_z^2 + \frac{1}{2}\langle D\rangle_{ij}(\hat{\Pi}_x\hat{\Pi}_y + \hat{\Pi}_y\hat{\Pi}_x) + \frac{i}{\hbar}\langle F\rangle_{ij}\hat{\Pi}_z \quad (2)$$

where E_i is the vibrational energy of state i, $\langle S\rangle_{ij}$ are the overlap integrals of states i and j, and $\hat{\Pi}_\alpha$ ($\alpha = x, y, z$) are the total angular momenta operators defined in the molecular coordinate system. The rotational constant matrices are defined as

$$\langle A\rangle_{ij} = \langle i|\mu_{xx}|j\rangle,\ \langle B\rangle_{ij} = \langle i|\mu_{yy}|j\rangle,\ \langle C\rangle_{ij} = \langle i|\mu_{zz}|j\rangle,\ \langle D\rangle_{ij} = \langle i|\mu_{xy}|j\rangle \quad (3)$$

These matrices (**A**−**D**) are symmetric. **F** represents the Coriolis coupling such that

$$\langle F\rangle_{ij} = \left\langle i\left|\frac{\hbar^2}{I'_{zz}}\left(t_3\frac{\partial}{\partial t_2} - t_2\frac{\partial}{\partial t_3}\right)\right|j\right\rangle \quad (4)$$

where $I'_{\alpha b}$ is the inertial tensor and $\mu_{\alpha\beta}$ is the inverse of $I'_{\alpha\beta}$. The elements of **F** are such that $\langle F\rangle_{ij} = -\langle F\rangle_{ji}$. The full rovibrational wave function was composed of a linear combination of pure vibrational wave functions and symmetric top eigenfunctions, $R^{\pm}_{JKM}$. Here H_{ij}^{VR} was subsequently diagonalized in the $R^{\pm}_{JKM}$ basis. By using $R^{\pm}_{JKM}$ basis functions, it was ensured that the corresponding matrix elements were real. The explicit form of these rovibrational functions has been detailed elsewhere[56] and as such will not be discussed further in the present work.

The potential energy integrals were determined using the Harris, Engerholm, and Gwinn (HEG) quadrature scheme.[60] The 1D vibrational eigenfunctions (i.e., the solutions of the 1D Schrödinger equation for a single t coordinate) were determined numerically using a finite-element method.[51] The full 3D eigenfunctions were then expanded as linear combinations of these 1D wave functions. In solving numerically the 3D vibrational Schrödinger equation, the expansion of the Watson operator[61] was truncated to third-order. The configuration weight of a particular vibrational state was calculated using the configuration coefficients C_{ijk}.[55]

The low-lying vibrational band origins (VBOs) of the ground states of $^7LiH_2^+$, $^7LiHD^+$, and $^7LiD_2^+$ are given in Table 4. The 1D domains used in the 3D integration were $t_1 = [-1.76\ a_0, +5.0\ a_0]$, $t_2 = [-0.648\ a_0, +4.0\ a_0]$, and $t_3 = [-4.0\ a_0, +4.0\ a_0]$. All 1D eigenvectors included in the configurational basis set decayed appropriately in the classical forbidden region of the potential.

The 3D vibrational wave functions were constructed using $n(t_1) \times n(t_2) \times n(t_3)$ configuration basis sets. Comparison of the lowest ten eigenvalues for ($^7LiH_2^+$,$^7LiD_2^+$) using the $10 \times 10 \times 10$, $15 \times 15 \times 15$, and $18 \times 18 \times 18$ vibrational configurational basis sets with those calculated using the $20 \times 20 \times 20$ basis set yielded standard deviations of (46.9 cm^{-1}, 43.3 cm^{-1}), (14.9 cm^{-1}, 13.5 cm^{-1}) and (4.4 cm^{-1}, 6.5 cm^{-1}), respectively. Such a comparison suggests that the vibrational eigenvalues calculated using the $20 \times 20 \times 20$ basis set have converged to within the residual error of the fitted potential energy function. Hence the vibrational states of $^{6,7}LiH_2^+$,$^{6,7}LiHD^+$, and $^{6,7}LiD_2^+$ were calculated using the $20 \times 20 \times 20$ basis set. Thus each vibrational wave function was composed of an 8000 term configuration interaction. All ^{6}Li data are available from the electronic archive.[54]

Table 4 also lists the assignments, irreducible representations and expansion densities of the dominant configuration components, and the vibrationally averaged equilibrium structures for

TABLE 4: Low-Lying Vibrational Band Origins, Their Respective Assignments, and Vibrationally Averaged Equilibrium Structures for the Electronic Ground States of $^7LiH_2^+$, $^7LiHD^+$, and $^7LiD_2^+$

$t_1t_2t_3$	symmetry	expansion density[a]	VBO[b]	$\langle R_{Li-H}\rangle$/Å	$\langle R_{Li-D}\rangle$/Å	$\langle\theta\rangle$/deg
		$^7LiH_2^+$				
|000⟩	a_1	0.80	0.0[c]	2.089		23.4
|100⟩	a_1	0.52	487.9	2.053		24.0
|001⟩	b_2	0.67	738.8	2.093		24.6
|200⟩,|100⟩	a_1	0.29, 0.22	1003.7	1.956		24.5
|101⟩,|001⟩	b_2	0.49, 0.10	1305.9	2.063		24.9
|200⟩,|300⟩,|500⟩	a_1	0.26, 0.15, 0.09	1550.8	2.200		24.6
|002⟩,|012⟩	a_1	0.48, 0.10	1586.1	2.089		25.1
|201⟩,|101⟩	b_2	0.18, 0.34	1891.3	1.925		25.4
|300⟩,|400⟩,|600⟩	a_1	0.28, 0.09, 0.09	2124.8	2.122		25.0
|102⟩,|112⟩	a_1	0.42, 0.08	2234.0	2.098		25.4
|301⟩,|201⟩	b_2	0.21, 0.19	2486.4	2.180		25.2
		$^7LiHD^+$				
|000⟩	a′	0.79	0.0[d]	2.100	2.096	20.6
|100⟩	a′	0.47	390.9	2.147	2.155	20.1
|001⟩	a″	0.58	640.9	2.116	2.113	19.4
|200⟩,|100⟩	a′	0.23, 0.22	805.1	2.179	2.180	19.9
|101⟩	a″	0.34	1067.1	2.141	2.138	19.2
|200⟩,|300⟩,|500⟩	a′	0.30, 0.10, 0.08	1248.3	2.203	2.195	19.9
|002⟩,|012⟩	a′	0.39, 0.08	1367.2	2.093	2.125	18.9
|201⟩, |101⟩	a″	0.18, 0.16	1532.3	2.163	2.151	19.2
|300⟩,|510⟩	a′	0.29, 0.05	1714.1	2.224	2.211	19.8
|102⟩,|112⟩	a′	0.22, 0.05	1837.1	2.115	2.131	18.9
|201⟩,|301⟩	a″	0.20, 0.10	2021.5	2.183	2.167	19.2
		$^7LiD_2^+$				
|000⟩	a_1	0.79	0.0[e]		2.094	20.6
|100⟩,|000⟩	a_1	0.46, 0.10	357.6		2.158	20.1
|001⟩	b_2	0.62	486.3		2.113	19.4
|100⟩,|200⟩,|400⟩	a_1	0.26, 0.20, 0.08	722.0		2.194	19.8
|101⟩,|001⟩	b_2	0.37, 0.15	880.3		2.152	19.3
|002⟩	a_1	0.45	1007.7		2.105	18.8
|200⟩,|300⟩	a_1	0.33, 0.07	1108.0		2.213	19.7
|101⟩,|201⟩	b_2	0.26, 0.19	1285.3		2.177	19.2
|102⟩,|002⟩	a_1	0.32, 0.10	1455.6		2.139	18.8
|300⟩, |400⟩,|510⟩	a_1	0.30, 0.09, 0.09	1515.7		2.227	19.7
|003⟩,|001⟩,|013⟩	b_2	0.31, 0.12, 0.10	1591.3		2.089	18.5

[a] Reference 55. [b] All values given in cm^{-1}. [c] $^7LiH_2^+$ zero-point energy = 2679.4 cm^{-1}. [d] $^7LiHD^+$ zero-point energy = 2324.8 cm^{-1}. [e] $^7LiD_2^+$ zero-point energy = 1918.0 cm^{-1}.

each vibrational state. The vibrational Hamiltonian[56] is fully anharmonic and so includes operators that couple the vibrational t coordinates. Therefore, vibrational states within the same irreducible representation may mix. In C_{2v} symmetry, a bound vibrational state is of b_2 symmetry if it includes odd quanta in the asymmetric stretch mode. Otherwise, all bound vibrational states are of a_1 symmetry. Similarly, in C_s symmetry all bound vibrational states belong to the a′ irreducible representation, except those with odd quanta in the asymmetric stretch mode.

In the case of $^7LiH_2^+$ configuration mixing was observed for several low-lying vibrational states. For example, the vibrational states with VBOs at 1003.7, 1305.9, 1586.1, 1891.3, 2234.0, and 2486.4 cm^{-1} were primarily composed of two configurations. In addition, the a_1 vibrational states with VBOs at 1550.8 and 2124.8 cm^{-1} were primarily composed of $0.26 \times |200\rangle + 0.15 \times |300\rangle + 0.09 \times |500\rangle$ and $0.28 \times |300\rangle + 0.09 \times |400\rangle + 0.09 \times |600\rangle$ configurations, respectively. As anticipated from the 1D vibrational calculations, low-lying bound vibrational states were composed mainly of linear combinations of 1D eigenfunctions in the t_1 and t_3 excited normal modes.

Configuration mixing was observed also in the low-lying vibrational states of $^7LiD_2^+$. For example, the vibrational states with VBOs at 357.6, 880.3, 1108.0, 1285.3, and 1455.6 cm^{-1} were composed primarily of two configurations. The b_2 state with VBO at 486.3 cm^{-1} and the a_1 state with VBO at 1007.7 cm^{-1} were found to be comprised mostly from a single configuration. Conversely, those states with VBOs at 722.0, 1515.7, and 1591.3 cm^{-1} were more delocalized, the major terms in these configurations being $0.26 \times |100\rangle + 0.20 \times |200\rangle + 0.08 \times |400\rangle$, $0.30 \times |300\rangle + 0.09 \times |400\rangle + 0.09 \times |510\rangle$, and $0.31 \times |003\rangle + 0.12 \times |001\rangle + 0.10 \times |013\rangle$, respectively. Using the multireference PES of Martinazzo et al.,[4] Bieske and co-workers[28] calculated the intermolecular stretch and bend frequencies of $^7LiD_2^+$ to be 365 and 503 cm^{-1}, respectively. The corresponding values calculated in the present work were comparable with these values, differing by ca. −7 and −17 cm^{-1}, respectively. For comparison, these same frequencies calculated by Bulychev et al.[22] were 329.8 and 447.2 cm^{-1}. Comparison of the lowest excited vibrational energies of $^7LiH_2^+$ calculated here with those calculated by Bulychev et al.[22] showed a similar trend. For instance, the energy of the lowest excited a_1 vibrational state of $^7LiH_2^+$ calculated here was ca. 88 cm^{-1} higher, and the energy of the lowest excited b_2 state calculated here was ca. 150 cm^{-1} higher. For the ground state of $^7LiD_2^+$, the vibrationally averaged D−D bond length was calculated to be 0.749 Å. This value is in excellent agreement with the D−D bond length calculated on the MRCI PES of Martinazzo et al.,[4] the latter being 0.751 Å.

As with $^7LiH_2^+$ and $^7LiD_2^+$, several low-lying excited vibrational states of $^7LiHD^+$ were composed of two primary configurations. Exceptions were found to be the lowest two a″ states, each ascribed to a single configuration, and the a′ state with VBO at 1248.3 cm^{-1}. The latter was found to consist mostly of a $0.30 \times |200\rangle + 0.10 \times |300\rangle + 0.08 \times |500\rangle$

TABLE 5: Rotational and Coriolis Matrix Elements of $^7LiH_2^+$, $^7LiHD^+$, and $^7LiD_2^+$ [a]

i	j	$^1/_2\langle A\rangle_{ij}$	$^1/_2\langle B\rangle_{ij}$	$^1/_2\langle C\rangle_{ij}$	$^1/_2\langle D\rangle_{ij}$	$\langle F\rangle_{ij}$
				$^7LiH_2^+$		
1	1	6.271+01	2.589+00	2.455+00	1.557−11	−2.198−17
2	1	5.554−01	3.679−01	3.332−01	−6.499−12	5.159−12
2	2	6.143+01	2.509+00	2.384+00	1.373−11	−5.358−17
3	1	5.752−11	−2.275−12	−2.244−12	−1.602+00	6.280−02
3	2	6.873−11	−3.783−13	−5.629−13	−1.152−01	9.739−01
3	3	7.215+01	2.617+00	2.449+00	−5.592−11	7.110−17
4	1	1.033+00	−7.696−02	−7.072−02	4.263−12	−4.479−12
4	2	-1.460+00	−4.955−01	−4.486−01	5.832−12	−6.830−12
4	3	−1.993−11	3.297−13	3.966−13	−2.340−01	3.317−01
4	4	6.032+01	2.491+00	2.366+00	1.110−11	−3.747−17
5	1	−6.973−12	−6.570−13	−5.707−13	−1.928−01	2.735−01
5	2	5.309−11	−9.321−13	−1.055−12	−1.475+00	4.756−03
5	3	2.492+00	3.532−01	3.131−01	3.850−12	−1.441−11
5	4	−7.677−11	−1.376−12	−1.003−12	2.273−01	−1.384+00
5	5	6.964+01	2.575+00	2.415+00	−5.096−11	3.135−17
				$^7LiHD^+$		
1	1	4.685+01	2.101+00	1.815+00	2.933+00	5.019−16
2	1	−3.186−01	2.142−01	2.305−01	−3.242−01	−1.078−04
2	2	4.689+01	2.044+00	1.761+00	2.946+00	−6.629−15
3	1	1.727+00	1.824−01	3.557−02	1.173+00	−3.000−02
3	2	−2.206+00	−4.504−02	−2.955−02	−1.195−01	−7.195−01
3	3	5.287+01	2.125+00	1.789+00	3.380+00	2.613−14
4	1	7.578−02	−5.932−02	−5.165−02	−1.032−02	7.270−03
4	2	−1.162−01	−3.042−01	−3.114−01	3.083−01	8.788−02
4	3	2.160−03	−4.451−03	-−1.694−02	1.100−01	−1.795−01
4	4	4.616+01	2.017+00	1.746+00	2.834+00	1.851−14
5	1	−2.445+00	2.889−03	3.249−03	−2.941−02	−2.042−01
5	2	1.676+00	1.510−01	1.063−02	1.151+00	−5.159−02
5	3	1.605−01	1.853−01	2.169−01	−4.451−01	1.787−01
5	4	1.848+00	3.866−02	3.771−02	−3.213−03	9.888−01
5	5	5.274+01	2.104+00	1.781+00	3.260+00	3.365−14
				$^7LiD_2^+$		
1	1	3.111+01	1.586+00	1.492+00	−5.314−11	−3.340−17
2	1	3.460−02	−2.031−01	−1.812−01	−5.7954−12	1.843−11
2	2	3.083+01	1.521+00	1.434+00	-5.019−11	2.221−19
3	1	−1.236−10	−1.811−12	−1.112−12	8.311−01	−5.428−03
3	2	−4.065−11	−1.699−12	−1.388−12	3.687−02	6.469−01
3	3	3.523+01	1.579+00	1.467+00	4.094−11	9.287−17
4	1	−3.797−01	4.423−02	4.006−02	1.191−12	−5.589−12
4	2	−2.879−01	−2.751−01	−2.450−01	−4.255−13	2.289−11
4	3	−2.416−11	−1.204−12	-9.977−13	−1.386−01	1.601−01
4	4	3.049+01	1.495+00	1.410+00	−2.655−11	1.421−17
5	1	−1.233−11	3.119−14	1.039−13	1.212−01	−1.121−01
5	2	1.002−10	1.825−13	−2.389−13	−7.715−01	−1.859−02
5	3	4.298−01	1.964−01	1.722−01	−4.849−12	9.728−12
5	4	1.799−11	4.942−12	4.387−12	2.544−02	−9.420−01
5	5	3.427+01	1.546+00	1.441+00	3.741−11	8.296−17

[a] All values given in cm^{-1}. **A**, **B**, **C**, **D**, and **F** matrix elements defined in eqs 3 and 4. 6.271+01 denotes 6.271×10^1.

configuration. Single excitations in the a′ bend mode were more prevalent in the low-lying vibrational levels of $^7LiHD^+$, because the a′ states with VBOs at 1367.2, 1714.1, and 1837.1 cm^{-1} each included such excitations.

The vibrationally averaged bond angle of the $^7LiH_2^+$ ground state was calculated to be 2.0° larger than the FCI optimized value. This has been ascribed to the presence of the a_1 bend mode of vibration in the overall vibrational CI. Isotopic substitution in the H−H molecular subunit had only a minor effect with respect to vibrationally averaged equilibrium structures. The effect of such substitution in $^7LiH_2^+$ is depicted in Figure 4 for the ground vibrational state.

The vibrationally averaged rotational and Coriolis matrix elements spanned by the lowest five vibrational states were calculated for $^7LiH_2^+$, $^7LiHD^+$, and $^7LiD_2^+$ and are given in Table 5. It is to be expected that elements of **F** would be small using an Eckart−Watson Hamiltonian. This was generally the case for the three isotopomers considered in the present work. For instance, the Coriolis matrix elements were generally found to be of the order of $10^{-11}-10^{-17}$, $10^{-14}-10^{-16}$, and $10^{-11}-10^{-17}$ cm^{-1} for $^7LiH_2^+$, $^7LiHD^+$, and $^7LiD_2^+$, respectively. The largest Coriolis matrix elements (in magnitude) for these respective species were calculated to be $\langle F\rangle_{32} = -1.384$ cm^{-1}, $\langle F\rangle_{54} = 9.888 \times 10^{-1}$ cm^{-1}, and $\langle F\rangle_{54} = -9.420 \times 10^{-1}$ cm^{-1}. The diagonal elements of **F** were at least 1 order of magnitude smaller relative to those off the diagonal in all cases, which was also anticipated.

The values of the ground state rotational constants and asymmetry parameters (κ) for $^7LiH_2^+$, $^7LiHD^+$, and $^7LiD_2^+$ were as anticipated. For instance, from Table 5 can be seen that $\langle B\rangle_{ii}$ and $\langle C\rangle_{ii}$ were in close agreement for the lowest five vibrational states. These values manifested themselves in κ values of $^7LiH_2^+$, $^7LiHD^+$, and $^7LiD_2^+$, which were calculated to be −0.996, −0.987, and −0.994, respectively. The rotational constants $\langle A\rangle_{11}$, $\langle B\rangle_{11}$, and $\langle C\rangle_{11}$ of $^7LiD_2^+$ calculated in the present work for $^7LiD_2^+$ also compared favorably with those corresponding to the equilibrium structure of Martinazzo et al.,[4] differing by +1.4, −0.2, and −0.2 cm^{-1}, respectively.

Several rovibrational transition frequencies in the D−D stretching band of $^7LiD_2^+$ (occurring at 2917.6 cm^{-1}) calculated in this work have been compared with recent experimental data.[28] This comparison is given in Table 6, for $K = 0$, 1, 2 and $J \leq 10$. From Table 6 it is observed that the agreement between these theoretical and experimental transition frequencies was better than ca. 5 cm^{-1} for the $K = 0$ and 1 manifolds, whereas for the $K = 2$ manifold the agreement was better than ca. 7 cm^{-1}. Using the data in Table 6, it was also possible to directly compare the FCI PEF via the rovibrational level spacings. It was observed that the spacing of all rovibrational levels in the D−D stretching band of $^7LiD_2^+$ for $K = 0$, 1, 2 and $J \leq 10$ were in good agreement with experimental data, with all the rovibrational transitions being larger than experiment. To summarize this comparison, the largest differences in the $K = 0$ manifold for the R and P branches were calculated to be 0.7 and 0.5 cm^{-1}, respectively. The largest differences here arose from the highest J values considered, viz. the $\Delta(9_{0,9} \leftarrow 8_{0,8}, 10_{0,10} \leftarrow 9_{0,9})$ and $\Delta(8_{0,8} \leftarrow 9_{0,9}, 9_{0,9} \leftarrow 10_{0,10})$ spacings. Similar differences were observed in the comparison of the level spacings for $K = 1$. For the $K = 1$ R, P, and Q branches respectively, the largest deviations in rovibrational level spacing from experiment were 0.7, 0.5, and 0.2 cm^{-1}, respectively. Within the $K = 2$ manifold, the largest difference in the R branch level spacings was 1.0 cm^{-1}, and for the P branch the largest difference was 0.6 cm^{-1}.

Rovibrational energies (for $v \leq 10$ and $J \leq 10$) and their respective assignments (in terms of J, K_a, K_c) of the $^{6,7}LiH_2^+$, $^{6,7}LiHD^+$, and $^{6,7}LiD_2^+$ ground states are available from the electronic archive.[54] The vibrationally averaged rotational and Coriolis matrix elements spanned by the lowest five vibrational states of $^6LiH_2^+$, $^6LiHD^+$, and $^6LiD_2^+$ are also available from the electronic archive.

4b. Radiative Properties. The approach of Sudarko and von Nagy-Felsobuki [59] has been employed to calculate the radiative properties of $^{6,7}LiH_2^+$, $^{6,7}LiHD^+$, and $^{6,7}LiD_2^+$. This method uses the quadrature scheme of HEG to construct the vibration transition moment integrals. Assuming that μ_α ($\alpha = x, y, z$) can be expanded as a power series in t coordinates, the vibration transition moment integrals are expressed in terms of the expectation value of the HEG quadrature points. As a result,

TABLE 6: Comparison of $^7LiD_2^+$ Rovibrational Transition Frequencies[a] for the D−D Stretch Band at 2906.1 cm^{-1} for $J \leq 10$

R branch				P branch				Q branch			
transition[b]	experiment	this work	Δ	transition[b]	experiment	this work	Δ	transition[b]	experiment	this work	Δ
					$K = 0$						
$1_{0,1} \leftarrow 0_{0,0}$	2917.7	2920.6	2.9	$0_{0,0} \leftarrow 1_{0,1}$	2911.5	2914.5	3.0				
$2_{0,2} \leftarrow 1_{0,1}$	2920.8	2923.7	2.9	$1_{0,1} \leftarrow 2_{0,2}$	2908.4	2911.4	3.0				
$3_{0,3} \leftarrow 2_{0,2}$	2923.8	2926.9	3.1	$2_{0,2} \leftarrow 3_{0,3}$	2905.3	2908.4	3.1				
$4_{0,4} \leftarrow 3_{0,3}$	2926.9	2930.0	3.1	$3_{0,3} \leftarrow 4_{0,4}$	2902.2	2905.4	3.2				
$5_{0,5} \leftarrow 4_{0,4}$	2929.9	2933.2	3.3	$4_{0,4} \leftarrow 5_{0,5}$	2899.1	2902.4	3.3				
$6_{0,6} \leftarrow 5_{0,5}$	2932.9	2936.4	3.5	$5_{0,5} \leftarrow 6_{0,6}$	2896.0	2899.5	3.5				
$7_{0,7} \leftarrow 6_{0,6}$	2935.8	2939.7	3.9	$6_{0,6} \leftarrow 7_{0,7}$	2892.9	2896.7	3.7				
$8_{0,8} \leftarrow 7_{0,7}$	2938.8	2943.0	4.2	$7_{0,7} \leftarrow 8_{0,8}$	2889.8	2893.9	4.1				
$9_{0,9} \leftarrow 8_{0,8}$	2941.6	2946.4	4.8	$8_{0,8} \leftarrow 9_{0,9}$	2886.7	2891.3	4.6				
$10_{0,10} \leftarrow 9_{0,9}$	2944.5	2949.9	5.4	$9_{0,9} \leftarrow 10_{0,10}$	2883.6	2888.7	5.1				
					$K = 1$						
$2_{1,2} \leftarrow 1_{1,1}$	2919.4	2922.3	2.9	$1_{1,0} \leftarrow 2_{1,2}$	2907.1	2910.3	3.2	$1_{1,1} \leftarrow 1_{1,0}$	2913.3	2916.1	2.8
$2_{1,1} \leftarrow 1_{1,0}$	2919.6	2922.5	2.9	$1_{1,1} \leftarrow 2_{1,2}$	2907.3	2910.2	2.9	$1_{1,0} \leftarrow 1_{1,1}$	2913.5	2916.3	2.8
$3_{1,3} \leftarrow 2_{1,2}$	2922.4	2925.4	3.0	$2_{1,1} \leftarrow 3_{1,2}$	2903.9	2906.9	3.0	$2_{1,2} \leftarrow 2_{1,1}$	2913.0	2916.0	3.0
$3_{1,2} \leftarrow 2_{1,1}$	2922.7	2925.7	3.0	$2_{1,2} \leftarrow 3_{1,3}$	2904.2	2907.2	3.0	$2_{1,1} \leftarrow 2_{1,2}$	2913.6	2916.5	2.9
$4_{1,4} \leftarrow 3_{1,3}$	2925.4	2928.5	3.1	$3_{1,2} \leftarrow 4_{1,3}$	2900.8	2903.9	3.1	$3_{1,3} \leftarrow 3_{1,2}$	2912.7	2915.8	3.1
$4_{1,3} \leftarrow 3_{1,2}$	2925.8	2928.9	3.1	$3_{1,3} \leftarrow 4_{1,4}$	2901.2	2904.3	3.1	$3_{1,2} \leftarrow 3_{1,3}$	2913.9	2916.9	3.0
$5_{1,5} \leftarrow 4_{1,4}$	2928.4	2931.6	3.2	$4_{1,3} \leftarrow 5_{1,4}$	2897.6	2900.9	3.3	$4_{1,3} \leftarrow 4_{1,4}$	2914.3	2917.4	3.1
$5_{1,4} \leftarrow 4_{1,3}$	2928.9	2932.1	3.2	$4_{1,4} \leftarrow 5_{1,5}$	2898.1	2901.4	3.3				
$6_{1,6} \leftarrow 5_{1,5}$	2931.3	2934.8	3.5	$5_{1,4} \leftarrow 6_{1,5}$	2894.5	2898.0	3.5				
$6_{1,5} \leftarrow 5_{1,4}$	2931.9	2935.4	3.5	$5_{1,5} \leftarrow 6_{1,6}$	2895.0	2898.5	3.5				
$7_{1,7} \leftarrow 6_{1,6}$	2934.2	2938.1	3.9	$6_{1,5} \leftarrow 7_{1,6}$	2891.3	2895.1	3.8				
$7_{1,6} \leftarrow 6_{1,5}$	2934.9	2938.8	3.9	$6_{1,6} \leftarrow 7_{1,7}$	2892.0	2895.8	3.8				
$8_{1,8} \leftarrow 7_{1,7}$	2937.1	2941.4	4.3	$7_{1,6} \leftarrow 8_{1,7}$	2888.2	2892.4	4.2				
$8_{1,7} \leftarrow 7_{1,6}$	2937.9	2942.2	4.3	$7_{1,7} \leftarrow 8_{1,8}$	2888.9	2893.1	4.2				
$9_{1,9} \leftarrow 8_{1,8}$	2939.9	2944.8	4.9	$8_{1,7} \leftarrow 9_{1,8}$	2885.1	2889.8	4.7				
$9_{1,8} \leftarrow 8_{1,7}$	2940.9	2945.8	4.9	$8_{1,8} \leftarrow 9_{1,9}$	2885.9	2890.5	4.6				
$10_{1,10} \leftarrow 9_{1,9}$	2942.7	2948.3	5.6	$9_{1,9} \leftarrow 10_{1,10}$	2882.9	2888.1	5.2				
$10_{1,9} \leftarrow 9_{1,8}$	2943.8	2949.4	5.6								
					$K = 2$						
$3_{2,2} \leftarrow 2_{2,1}$	2918.8	2922.4	3.6	$2_{2,0} \leftarrow 3_{2,1}$	2900.3	2903.9	3.6				
$3_{2,1} \leftarrow 2_{2,0}$	2918.8	2922.4	3.6	$2_{2,1} \leftarrow 3_{2,2}$	2900.3	2903.9	3.6				
$4_{2,3} \leftarrow 3_{2,2}$	2921.8	2925.6	3.8	$3_{2,1} \leftarrow 4_{2,2}$	2897.3	2901.0	3.7				
$4_{2,2} \leftarrow 3_{2,1}$	2921.8	2925.6	3.8	$3_{2,2} \leftarrow 4_{2,3}$	2897.3	2901.0	3.7				
$5_{2,4} \leftarrow 4_{2,3}$	2924.8	2928.9	4.1	$4_{2,2} \leftarrow 5_{2,3}$	2894.2	2898.2	4.0				
$5_{2,3} \leftarrow 4_{2,2}$	2924.8	2928.9	4.1	$4_{2,3} \leftarrow 5_{2,4}$	2894.2	2898.2	4.0				
$6_{2,5} \leftarrow 5_{2,4}$	2927.8	2932.3	4.5	$5_{2,3} \leftarrow 6_{2,4}$	2891.1	2895.4	4.3				
$6_{2,4} \leftarrow 5_{2,3}$	2927.8	2932.3	4.5	$5_{2,4} \leftarrow 6_{2,5}$	2891.1	2895.4	4.3				
$7_{2,6} \leftarrow 6_{2,5}$	2930.8	2935.8	5.0	$6_{2,4} \leftarrow 7_{2,5}$	2888.0	2892.8	4.8				
$7_{2,5} \leftarrow 6_{2,4}$	2930.8	2935.8	5.0	$6_{2,5} \leftarrow 7_{2,6}$	2888.0	2892.8	4.8				
$8_{2,7} \leftarrow 7_{2,6}$	2933.7	2939.4	5.7	$7_{2,5} \leftarrow 8_{2,6}$	2884.9	2890.3	5.4				
$8_{2,6} \leftarrow 7_{2,5}$	2933.7	2939.4	5.7	$7_{2,6} \leftarrow 8_{2,7}$	2884.9	2890.3	5.4				
$9_{2,8} \leftarrow 8_{2,7}$	2936.6	2943.1	6.5								
$9_{2,7} \leftarrow 8_{2,6}$	2936.6	2943.2	6.6								
$10_{2,9} \leftarrow 9_{2,8}$	2939.5	2947.1	7.6								
$10_{2,8} \leftarrow 9_{2,7}$	2939.5	2947.1	7.6								

[a] All values given in cm^{-1}. Experimental data from reference 28. [b] Transitions assigned using the J, K_a, K_c scheme.

the transition integrals may be calculated at points on the HEG quadrature grid in the same manner as the potential energy integrals.

The vibrational band origins, square dipole matrix elements, Einstein A and B coefficients, band strengths, and radiative lifetimes of the $^7LiH_2^+$, $^7LiHD^+$, and $^7LiD_2^+$ electronic ground states are presented in Table 7. These radiative properties were also calculated for the $^6LiH_2^+$, $^6LiHD^+$, and $^6LiD_2^+$ ground states, the results of which are available from the electronic archive.[54]

The rovibrational transition probability between an initial rovibrational state $|a\rangle$ and a final state $|b\rangle$ is given as[59]

$$R_{ab}{}^2 = \sum_{M_1} \sum_{M_w} |\langle \Psi_{V_a J_a K_a M_a} | \mu_{SF} | \Psi_{V_b J_b K_b M_b} \rangle|^2 \qquad (5)$$

where $\Psi_{V_a J_a K_a M_a}$ is the rovibrational wave function of state $|a\rangle$, and μ_{SF} is the dipole moment operator transformed to the spaced-fixed frame. The corresponding spectral line intensity is given by[62]

$$S_{ab} = \frac{8\pi^3}{3hc} \frac{C_A N_A}{Q_V Q_R} \frac{g_{nsi}}{RT} \upsilon_{ab} [e^{-hcEa/kT} - e^{-hcEb/kT}] R_{ab}{}^2 \qquad (6)$$

where C_A is the molecular isotopic abundance, g_{nsi} is the nuclear statistical weight of state $|a\rangle$, υ_{ab} is the transition frequency (cm^{-1}) of the $V_a \rightarrow V_b$ vibrational transition, E_a and E_b are the energies (cm^{-1}) of the respective rovibrational states, and Q_V and Q_R are the vibrational and rotational partition functions, respectively. Here N_A, h, c, R, T, and k are defined here in the usual manner.[63]

Rovibrational transition frequencies, spectral line intensities and their respective assignments of the $^{6,7}LiH_2^+$, $^{6,7}LiHD^+$, and $^{6,7}LiD_2^+$ electronic ground states were calculated for $\upsilon \leq 4$ and $J \leq 4$ and $T = 296$ K. It should be noted that the J selection

TABLE 7: Vibrational Band Origins υ_{ij}, Square Dipole Matrix Elements R^2, Einstein Coefficients (A_{ji}, B_{ji}), Band Strengths S_{ji}, and Radiative Lifetimes τ of the $^7LiH_2^+$, $^7LiHD^+$, and $^7LiD_2^+$ Ground States,[a] Calculated at 296 K

j	i	υ_{ij}/cm^{-1}	R^2/au^2	A_{ji}/s^{-1}	B_{ji}/10^{16} cm^3 erg^{-1} s^2	S_{ji}/cm molecule^{-1}	τ/s
				$^7LiH_2^+$ [b]			
1	0	487.9	2.34+01	8.54+02	4.42+03	3.87−15	6.42−04
2	0	738.8	3.59+01	4.54+03	6.76+03	9.61−15	1.91−04
3	0	1003.7	2.33+00	7.39+02	4.39+02	8.66−16	2.00−04
4	0	1305.9	1.73+01	1.21+04	3.25+03	8.39−15	3.55−05
5	0	1550.8	3.49−01	4.09+02	6.58+01	2.02−16	7.70−05
6	0	1586.1	2.73+00	3.42+03	5.14+02	1.60−15	4.40−05
7	0	1891.3	1.30+00	2.75+03	2.45+02	9.15−16	1.37−05
8	0	2124.8	4.54−02	1.37+02	8.56+00	3.60−17	3.66−05
9	0	2234.0	8.59−01	3.00+03	1.62+02	7.15−16	1.11−05
10	0	2486.4	9.11−01	4.39+03	1.72+02	8.44−16	7.38−06
				$^7LiHD^+$ [c]			
1	0	390.9	1.88+01	3.52+02	3.54+03	2.15−15	1.02−03
2	0	640.9	3.15+01	2.61+03	5.94+03	6.66−15	3.03−04
3	0	805.1	3.80+00	6.22+02	7.16+02	1.03−15	3.18−04
4	0	1067.1	7.89+00	3.01+03	1.49+03	2.89−15	9.39−05
5	0	1248.3	4.10−01	2.50+02	7.72+01	1.76−16	1.25−04
6	0	1367.2	6.77+00	5.42+03	1.27+03	3.18−15	5.21−05
7	0	1532.3	5.78−01	6.52+02	1.09+02	3.05−16	3.61−05
8	0	1714.1	4.20−02	6.63+01	7.91+00	2.48−17	6.11−05
9	0	1837.1	3.34−01	6.50+02	6.29+01	2.12−16	2.44−05
10	0	2021.5	2.08−01	5.38+02	3.91+01	1.45−16	1.78−05
				$^7LiD_2^+$ [d]			
1	0	357.6	1.76+01	2.53+02	3.32+03	1.65−15	1.17−03
2	0	486.4	2.41+01	8.69+02	4.53+03	3.36−15	6.75−04
3	0	722.0	1.36+00	1.61+02	2.57+02	3.03−16	4.63−04
4	0	880.3	1.07+01	2.30+03	2.02+03	2.95−15	1.45−04
5	0	1007.7	1.90−01	6.10+02	3.58+02	6.03−16	1.82−04
6	0	1108.0	1.29−03	5.49−01	2.42−01	4.50−19	2.19−04
7	0	1285.3	4.60−01	3.06+02	8.66+01	1.87−16	5.97−05
8	0	1455.6	3.70−01	3.58+02	6.97+01	1.71−16	4.72−05
9	0	1515.8	2.25−04	2.46−01	4.24−02	1.08−19	1.13−04
10	0	1591.3	3.10+00	3.92+03	5.84+02	1.56−15	5.35−05

[a] 2.34+01 denotes 2.34×10^1. [b] $^7LiH_2^+$ zero−point energy = 2679.4 cm^{-1}. [c] $^7LiHD^+$ zero−point energy = 2324.8 cm^{-1}. [d] $^7LiD_2^+$ zero−point energy = 1918.0 cm^{-1}.

rules can be disregarded here, because values of R_{ab}^2 have been calculated exactly (that is, using the "full" rovibrational wave function and the spatially transformed DMF). These rovibrational transitions and line strengths are shown in Figures 5 and 6 for the ^7Li and ^6Li species, respectively, using a line intensity threshold of 1.0×10^{-30} cm molecule^{-1}. The 305, 514, and 233 transitions are shown for the $^7LiH_2^+$, $^7LiHD^+$, and $^7LiD_2^+$ ground states, respectively, and for $^6LiH_2^+$, $^6LiHD^+$, and $^6LiD_2^+$ 302, 507, and 215 transitions are shown.

It was observed that the $^7LiH_2^+$ ground state possessed the most intense rovibrational transitions of the three ^7Li species, the most intense of which has been assigned to the $2_{02} \leftarrow 3_{03}$ transition of the $|001\rangle$ band (ω_{ab}= 754.1 cm^{-1}, $S_{ab} = 2.12 \times 10^{-17}$ cm molecule^{-1}). The $^7LiHD^+$ and $^7LiD_2^+$ ground states also exhibited their most intense bands for the $2_{02} \leftarrow 3_{03}$ rotational transition in the $|001\rangle$ band. These transitions occurred at 651.8 and 495.4 cm^{-1} with spectral line intensities of 1.47×10^{-20} and 3.72×10^{-25} cm molecule^{-1}, respectively. From Figure 6 it can be seen that among the ^6Li species, $^6LiH_2^+$ possessed the most intense rovibrational transitions. The most intense transition of $^6LiH_2^+$ was assigned to the $2_{02} \leftarrow 3_{03}$ rotational transition in the $|001\rangle$ band, for which ω_{ab} and S_{ab} were 856.8 cm^{-1} and 8.43×10^{-18} cm molecule^{-1}, respectively. This transition was also found to be the most intense for $^6LiHD^+$ and $^6LiD_2^+$. For the $2_{02} \leftarrow 3_{03}$ transition in the $|001\rangle$ band of $^6LiHD^+$, ω_{ab}= 653.4 cm^{-1}, $S_{ab} = 1.71 \times 10^{-21}$ cm molecule^{-1}, whereas ω_{ab} and S_{ab} for the $2_{02} \leftarrow 3_{03}$ transition in the $|001\rangle$ band of $^6LiD_2^+$ were 496.3 cm^{-1} and 6.59×10^{-26} cm molecule^{-1}, respectively.

5. Conclusions

Ab initio vibrational and rovibrational energies and radiative properties of the $^{6,7}LiH_2^+$, $^{6,7}LiHD^+$, and $^{6,7}LiD_2^+$ ground states have been calculated. Rovibrational energies were calculated using a FCI PEF embedded in an Eckart−Watson molecular Hamiltonian.[56] The radiative properties, including the rovibrational transition intensities, were calculated using a FCI DMF transformed to the space-fixed frame. The single particle basis sets used in the construction of the discrete PES and DMS reliably reproduced the properties of Li^+, Li, $^7LiH^+$, ^7LiH, and H_2. In all rovibrational calculations, molecular integrals were calculated using an adapted HEG scheme.[60] The rovibrational states and transitions have been assigned using a scheme described previously.[55] Molecular parameters and low-lying rovibrational energies of $^7LiD_2^+$ were observed to be in close agreement with both recent theory[4] and experiment.[28] Additionally, rovibrational transition frequencies in the D−D stretch band of $^7LiD_2^+$ calculated using this method were in excellent agreement with experimentally observed values.[28] It is hoped that the calculated rovibrational transition frequencies and their respective spectral line intensities will provide an aid to the experimental detection of the $^{6,7}LiH_2^+$, $^{6,7}LiHD^+$, and $^6LiD_2^+$ ground states.

Acknowledgment. We acknowledge support given by Australian Partnership for Advanced Computing, Australian Centre for Advanced Computing and Communications, the Australian Research Council and the Research Committee of The University of Newcastle. A.J.P. acknowledges support from

the Australian Post-Graduate Scholarship Scheme, and Mr. David Huthnance for computing support. E.v.N.F. acknowledges the Research School of Chemistry at the Australian National University for support during his sabbatical leave.

Supporting Information Available: Electronic versions of the FCI CVTZ(Li)/aug-cc-pVTZ(H) PES and DMS of the $^7LiH_2^+$ ground state are available. The PES and DMS consist of 83 and 47 discrete ab initio points respectively. Electronic versions of the lowest 10 vibrational and rovibrational states of the $^7LiH_2^+$, $^7LiHD^+$ and $^7LiD_2^+$ ground states and their J, K_a, K_c assignments are also available. These data consist of 1200 rovibrational levels for each species. The vibrational band origins, assignments, and vibrationally averaged structures of $^6LiH_2^+$, $^6LiHD^+$, and $^6LiD_2^+$, as well as the rotational constant matrices, vibrational radiative properties, and the rovibrational states and assignments for the lowest 10 vibrational and rotational levels are also available electronically. This material is available free of charge via the Internet at http://pubs.acs.org.

References and Notes

(1) Gianturco, F. A.; Gori Giorgi, P.; Berriche, H.; Gadea, F. X. *Astron. Astrophys. Suppl. Ser.* **1996**, *117*, 377.
(2) Lepp, S.; Shull, J. M. *Astrophys. J.* **1984**, *280*, 465.
(3) Bodo, E.; Gianturco, F. A.; Martinazzo, R.; Raimondi, M. *J. Phys. Chem. A* **2001**, *105*, 10986.
(4) Martinazzo, R.; Tantardini, G. F.; Bodo, E.; Gianturco, F. A. *J. Chem. Phys.* **2003**, *119*, 11241.
(5) Martinazzo, R.; Bodo, E.; Gianturco, F. A.; Raimondi, M. *Chem. Phys.* **2003**, *287*, 335.
(6) Sanz, C.; Bodo, E.; Gianturco, F. A. *Chem. Phys.* **2005**, *314*, 135.
(7) Searles, D. J.; von Nagy-Felsobuki, E. I. *Phys. Rev. A* **1991**, *43*, 3365.
(8) Wu, C. H. *J. Chem. Phys.* **1979**, *71*, 783.
(9) Sug Lee, H.; Sup Lee, Y.; Jeung, G.-H *J. Phys. Chem. A* **1999**, *103*, 11080.
(10) Davy, R.; Skoumbourdis, E.; Kompanchenko, T. *Mol. Phys.* **1999**, *97*, 1263.
(11) Russek, A.; Snyder, R.; Furlan, R. J. *Phys. Rev. A* **1989**, *39*, 6158.
(12) Dixon, D. A.; Gole, J. L.; Komornicki, A. *J. Phys. Chem.* **1988**, *92*, 1378.
(13) Cardelino, B. H.; Eberhardt, W. H.; Borkman, R. F. *J. Chem. Phys.* **1986**, *84*, 3230.
(14) Hobza, P.; Schleyer, P. v. R. *Chem. Phys. Lett.* **1984**, *105*, 630.
(15) Collins, J. B.; Schleyer, P. v. R.; Binkley, J. S.; Pople, J. A.; Radom, L. *J. Am. Chem. Soc.* **1976**, *98*, 3436.
(16) Kochanski, E. *Chem. Phys. Lett.* **1974**, *28*, 471.
(17) Raffenetti, R. C.; Ruedenberg, K. *J. Chem. Phys.* **1973**, *59*, 5978.
(18) Lester, W. A. *J. Chem. Phys.* **1971**, *54*, 3171.
(19) Lester, W. A. *J. Chem. Phys.* **1970**, *53*, 1511.
(20) Ray, N. K. *J. Chem. Phys.* **1970**, *52*, 463.
(21) Wu, A.-J.; Ellison, F. O. *J. Chem. Phys.* **1967**, *47*, 1458.
(22) Bulychev, V. P.; Bulanin, K. M.; Bulanin, M. O. *Opt. Spectrosc.* **2004**, *96*, 205.
(23) Huzinaga, S. *J. Chem. Phys.* **1965**, *43*, 1293.
(24) Kutzelnigg, W.; Staemmler, V.; Hoheisel, C. *Chem. Phys.* **1973**, *1*, 27.
(25) Xiao, Y.; Poirier, B. *J. Chem. Phys.* **2005**, *122*, 124318.
(26) Taylor, B. K.; Hinde, R. J. *J. Chem. Phys.* **1999**, *111*, 973.
(27) Taylor, B. K.; Hinde, R. J. *J. Chem. Phys.* **2005**, *122*, 074308.
(28) Thompson, C. D.; Emmeluth, C.; Poad, B. L. J.; Weddle, G. H.; Bieske, E. J. *J. Chem. Phys.* **2006**, *125*, 044310.
(29) Knowles, P. J.; Handy, N. C. *Chem. Phys. Lett.* **1984**, *111*, 315.
(30) Knowles, P. J.; Handy, N. C. *Comput. Phys. Commun.* **1989**, *54*, 75.
(31) Amos, R. D.; Bernhardsson, A.; Berning, A.; Celani, P.; Cooper, D. L.; Deegan, M. J. O.; Dobbyn, A. J.; Eckert, F.; Hampel, C.; Hetzer, G.; Knowles, P. J.; Korona, T.; Lindh, R.; Lloyd, A. W.; McNicholas, S. J.; Manby, F. R.; Meyer, W.; Mura, M. E.; Nicklass, A.; Palmieri, P.; Pitzer, R.; Rauhut, G.; Schütz, M.; Schumann, U.; Stoll, H.; Stone, A. J.; Tarroni, R.; Thorsteinsson, T.; Werner, H.-J. MOLPRO 2002.6.
(32) Page, A. J.; Wilson, D. J. D.; von Nagy-Felsobuki, E. I. *Chem. Phys. Lett.* **2006**, 335.
(33) Iron, M. A.; Oren, M.; Martin, J. M. L. *Mol. Phys.* **2003**, *101*, 1345.
(34) Dunning, T. H., Jr. *J. Chem. Phys.* **1989**, *90*, 1007.
(35) Sansonetti, J. E.; Martin, W. C. *J. Phys. Chem. Ref. Data* **2005**, *34*.
(36) Magnier, S. *J. Phys. Chem. A* **2004**, *108*, 1052.
(37) Dulick, M.; Zhang, K.-Q.; Guo, B.; Bernath, P. F. *J. Mol. Spectrosc.* **1998**, *188*, 14.
(38) Chan, Y. C.; Harding, D. R.; Stwalley, W. C.; Vidal, C. R. *J. Chem. Phys.* **1986**, *85*, 2436.
(39) Rothstein, E. *J. Chem. Phys.* **1969**, *50*, 1899.
(40) Balakrishnan, A.; Smith, V.; Stoicheff, B. P. *Phys. Rev. Lett.* **1991**, *68*, 2149.
(41) Dalgarno, A.; Kirby, K.; Stancil, P. C. *Astrophys. J.* **1996**, *458*, 397.
(42) Berriche, H.; Gadea, F. X. *Chem. Phys. Lett.* **1996**, *203*.
(43) Votjik, J.; Cespiva, L.; Savrda, J.; Paidarova, I. *J. Mol. Spectrosc.* **1990**, *142*, 279.
(44) Huber, K. P.; Herzberg, G. *Mol. Spectrosc. Mol. Struct.* **1978**, *4*.
(45) Yang, C.-L.; Huang, Y.-J.; Zhang, X.; Han, K.-L. *THEOCHEM* **2003**, *625*, 289.
(46) Woon, D. E.; Dunning, T. H., Jr. *J. Chem. Phys.* **1993**, *98*, 1358.
(47) Kendall, R. A.; Dunning, T. H., Jr.; Harrison, R. J. *J. Chem. Phys.* **1992**, *96*, 6796.
(48) Peterson, K. A.; Woon, D. E.; Dunning, T. H., Jr. *J. Chem. Phys.* **1994**, *100*, 7410.
(49) Wilson, A.; van Mourik, T.; Dunning, T. H., Jr. *THEOCHEM* **1997**, *388*, 339.
(50) Schmidt, M. W.; Baldridge, K. K.; Boatz, J. A.; Elbert, S. T.; Gordon, M. S.; Jensen, J. H.; Koseki, S.; Matsunaga, N.; Nguyen, K. A.; Su, S. J.; Windus, T. L.; Dupuis, M.; Montgomery, J. A. GAMESS: General Atomic and Molecular Electronic Structure System.
(51) Searles, D. J.; von Nagy-Felsobuki, E. I. *Am. J. Phys.* **1988**, *56*, 444.
(52) Searles, D. J.; von Nagy-Felsobuki, E. I. *Comput. Phys. Commun.* **1992**, *67*, 527.
(53) Hughes, J. M.; von Nagy-Felsobuki, E. I. *J. Mol. Struct. (THEOCHEM)* **1997**, *389*, 1.
(54) Electronic versions of the FCI CVTZ(Li)/aug-cc-pVTZ(H) 83-point LiH_2^+ PES, 47-point LiH_2^+ DMS, and vibrational/rovibrational states of the LiH_2^+, $LiHD^+$, and LiD_2^+ ground states are available as Supporting Information, free of charge via the internet at http://pubs.acs.org.
(55) Searles, D. J.; von Nagy-Felsobuki, E. I. Ab initio Variational Calculations of Molecular Vibrational-Rotational Spectra. In *Lecture Notes in Chemistry*; Springer-Verlag: Berlin, 1993; Vol. 61.
(56) Carney, G. D.; Langhoff, S. R.; Curtiss, L. A. *J. Chem. Phys.* **1977**, *102*, 5570.
(57) Eckart, C. *Phys. Rev.* **1935**, *47*, 552.
(58) Gabriel, W.; Reinsch, E.-A; Rosmus, P.; Carter, S.; Handy, N. C. *J. Chem. Phys.* **1993**, *99*, 897.
(59) Sudarko; Hughes, J. M.; von Nagy-Felsobuki, E. I. *Aust. J. Phys.* **2000**, *53*, 665.
(60) Harris, D. O.; Engerholm, G. G.; Gwinn, W. D. *J. Chem. Phys.* **1965**, *43*, 1515.
(61) Watson, J. K. G. *Mol. Phys.* **1968**, *15*, 479.
(62) Sudarko; von Nagy-Felsobuki, E. I. *Phys. Chem. Chem. Phys.* **2004**, *6*, 4542.
(63) Mohr, P. J.; Taylor, B. N. *Rev. Mod. Phys.* **2002**, *77*, 1.